LRP 542/96 March 1996

OPERATION OF A QUASI-OPTICAL GYROTRON WITH A GAUSSIAN OUTPUT COUPLER

J.P. Hogge, T.M. Tran, P.J. Paris, M.Q. Tran

submitted for publication in

PHYSICS OF PLASMAS

Operation of a quasi-optical gyrotron with a gaussian output coupler

J.P. Hogge*, T.M. Tran, P.J. Paris and M.Q. Tran,
Centre de Recherches en Physique des Plasmas,
Association Euratom - Confédération Suisse,
Ecole Polytechnique Fédérale de Lausanne,
21, Avenue des Bains, CH-1007 Lausanne, Switzerland
(March 1, 1996)

Abstract

The operation of a 92 GHz quasi-optical gyrotron (QOG) having a resonator formed by a spherical mirror and a diffraction grating placed in -1 order Littrow mount is presented. A power of 150 kW with a gaussian output pattern was measured. The gaussian content in the output was 98% with less than 1% of depolarization. By optimizing the magnetic field at fixed frequency, a maximum efficiency of 15% was reached.

I. INTRODUCTION

High-power transmission lines used for Electron Cyclotron Resonance Heating of fusion plasma require a gaussian input beam to maximize the coupling efficiency to the HE_{11} mode of the corrugated waveguide and to minimize the losses [1]. For cylindrical gyrotrons, a solution is provided by quasi-optical mode converters [2]. In a QOG, the electron beam interacts with the gaussian $TEM_{0,0,q}$ resonant mode of a Fabry-Pérot cavity formed by two spherical mirrors placed perpendicularly to the electron beam path [3]. The microwave power is usually extracted from the resonator by diffraction around the edges and then directed into an overmoded waveguide. Cold and hot tests indicated that the output does not correspond to any well-defined mode, rendering its subsequent conversion into a HE_{11} mode extremely inefficient [4]. The coupling efficiency to a corrugated waveguide or to a gaussian beam is estimated to be lower than 50%.

A method has been proposed to obtain a gaussian output from a QOG [5]. It consists in replacing one of the spherical mirrors by a diffractive grating placed in -1 order Littrow mount. The direction of the -1 order of diffraction coincides with the incident direction, providing the necessary feedback into the resonator. The grating can be considered as a smooth reflector for the 0 order of diffraction, through which the energy is extracted from the cavity. The electromagnetic field profile in the 0 order is the image of the pattern inside the cavity and is therefore gaussian.

The design principles of these grating couplers and their cold test performances are described in detail in Ref. [6] and will be only briefly summarized in section II. A cavity designed under these principles was implemented in a QOG and tested at high power levels ($P_{RF} = 150$ kW, $f_{RF} = 92$ GHz). The experimental set-up and the diagnostics are described at section III.

The main focus of the experiment was the output pattern of the gyrotron, but other properties related to the interaction between the electromagnetic waves and the electron beam cavity were measured and are presented at section IV. Due to the frequency dependence of the quality factor $Q(q)$ versus the cavity longitudinal $TEM_{0,0,q}$ modes, oscillation in a given longitudinal mode q is favored: the static magnetic field B_z can be used to optimize the output power. This is the first time that this well established procedure for cylindrical cavity gyrotrons is applied to a QOG. Due to the fact that $Q(q)$ is weakly dependent on q in the case of a conventional Fabry-Pérot resonator, longitudinal mode jumping occurs and the corresponding range optimization is narrow.

II. DESIGN OF THE GRATING COUPLER

The main steps of the design of the grating are described in Ref. [6] and can be outlined as follows:

a. Select the parameters (waist, spot size, spot size on the mirrors, output power transmission) of the cavity gaussian-like resonant mode, taking into account the gyrotron interaction constraints.

b. Knowing the designed output power transmission (i.e. the fraction of incident energy which is diffracted at 0 order (typically 1%-10%), determine the optimal incidence angle and the orientation of the grooves with respect to the electric field based on the electromagnetic

theory of gratings [7]. A sinusoidal groove profile was chosen to minimize the risk of arcing on the grating surface. Under these conditions, the best groove orientation is TM (electric field of the incident beam perpendicular to the grooves) and the normalized groove spacing h/d and incidence angle θ are:

$$h/d \sim 0.3, \theta \sim 25^o \tag{1}$$

where h is the groove depth and d the groove spacing.

c. The -1 order Littrow condition is automatically satisfied if the groove distribution is taken as the intersection of wavefronts of the incident microwave beam separated in phase by π and the surface supporting the grating. Applied to a resonator, this condition ensures that the phasefronts of the resonant mode are correctly reconstructed upon diffraction at the order -1.

d. An ellipsoid was chosen as grating support. With this choice the depolarization associated with the mixed TE (electric field parallel to the grooves) and TM incidence on parts of the grating was minimized. The output beam waist could also be adjusted to match the optimal diameter for coupling into an HE_{11} corrugated waveguide.

We define the gaussian content C^2 and the fraction of depolarized power XP as:

$$C^2 = \frac{\left[\int_{\Sigma_0} \sqrt{S_x}\, \exp\left\{-\frac{x'^2+y'^2}{w'^2}\right\} dx'\, dy'\right]^2}{\left[\int_{\Sigma_0} S_x\, dx'\, dy'\right]\, \left[\int_{\Sigma_0} \exp\left\{-\frac{2(x'^2+y'^2)}{w'^2}\right\} dx'\, dy'\right]} \tag{2}$$

and

$$XP = \frac{\int_{\Sigma_0} S_y\, dx'\, dy'}{\int_{\Sigma_0} S_x\, dx'\, dy' \; + \; \int_{\Sigma_0} S_y\, dx'\, dy'} \tag{3}$$

where z is the direction of propagation of the output beam and w' is a fit parameter. The quantities S_x and S_y represent respectively the z-component of the Poynting vector associated with the electric field in the x and y-direction

$$S_x = \frac{\left|\mathrm{Re}\left[E_x^0 \cdot B_y^{0*}\right]\right|}{\mu_0} \tag{4}$$

$$S_y = \frac{\left|\mathrm{Re}\left[E_y^0 \cdot B_x^{0*}\right]\right|}{\mu_0} \tag{5}$$

The phase is not taken into account in formulae 2 and 3. S_x and S_y are directly related to the square root of the signal measured with the receptive horn sensitive to the x-polarization (correct polarization) and to the y-polarization (cross-polarization or depolarization).

With these parameters, numerical simulations indicate that an output beam gaussian content as high as 99% with depolarization losses of the order of 3% can be expected.

The gaussian content as well as the quality factor Q of the resonator are maximized for a specific mode of longitudinal index $q = q_0$, which will be called the central mode. The output pattern associated to adjacent modes ($q = q_0 \pm 1, 2 \ldots$) is slightly distorted and they propagate along shifted axes. It is possible to adjust the index of the central mode within a few GHz bandwidth without significant change of its quality factor by mean of a rotation of the diffraction grating [8].

III. EXPERIMENTAL SET-UP

A. The QOG

The schematic of the QOG is presented in Fig.1. The static magnetic field B_z (where z is now and for the rest of the paper the magnetic field axis) was produced by a pair of superconducting coils operating at fields up to 4.1 T. The design frequency was 92.4 GHz. Two copper coils were placed in the region of the electron gun to adjust the magnetic field and its gradient in the gun. The magnetic profile in the vicinity of the interaction was double-humped with a ratio of the maximal field over the field in the interaction region $B_{max}/B_{z_0} = 1.11$.

The triode MIG gun was operated at a cathode voltage between 70 kV and 76 kV, a modulation anode voltage from 20 kV to 27 kV and a beam current up to 15 A. The electron beam pitch factor α could be varied between 1 and 1.3. The beam tunnel consisted of an alternance of copper rings (internal diameter 10 mm) and rings made of absorbing ceramic (MgOSiC with 95% MgO and 5% SiC). The drift length between the gun and the interaction region was 57 cm. Table I gives the computed beam parameters in the interaction region at 14 A using DAPHNE [9]. The potential depression associated with the gap of the interaction region (44 mm) was estimated around 6.8 kV for a cathode voltage $V_k = 70$ kV and $I_b = 14$ A.

Since the cross bore diameter was only 104 mm, the grating had to be placed in a vacuum vessel adjacent to the cryostat. The interaction length was $kw_{01} = 20$, where k is the wavenumber and w_{01} is the beam waist of the resonant modes. The curvature parameter of the equivalent resonator was $g = \mathrm{sign}(g_1)\sqrt{g_1 g_2} = -0.7$, where $g_i = 1 - D/R_i$, D being the mirror separation and R_i the radius of curvature of mirror i. These parameters were chosen in order to optimize the gyrotron interaction while minimizing the peak ohmic heat load on the mirrors of the equivalent resonator [10].

The equivalent Fresnel number of the grating was approximately $N = 2$. The diffraction losses around the edges were negligible for the central $\mathrm{TEM}_{0,0,q_0}$ mode and the quality factor Q of a resonance could be related to the fraction e_0 of power diffracted at the order 0 by

$$e_0 \simeq \frac{4\pi D}{Q\lambda}, \tag{6}$$

where λ is the wavelength. The diffraction losses around the edges of the grating for higher order transversal modes ($\mathrm{TEM}_{l,p,q}$, $l \geq 0$ or $p \geq 0$ were at least one order of magnitude higher than the one of the $\mathrm{TEM}_{0,0,q}$ mode: these modes were not observed during the gyrotron operation.

The angle of incidence θ on the grating and the normalized sinusoidal groove depth h/d were $\theta = 28^o$ and $h/d = 0.35$. This resulted in a power efficiency at the order 0 for the TM case $e_{0_{TM}} = 4\%$, and for the TE case $e_{0_{TE}} = 34\%$. TE polarization could therefore not be excited. With the above grating parameters there was no resonance at the second harmonic of the cyclotron frequency, even though the grating was in -2 order Littrow mount for $\omega = 2\Omega$.

The semi-axes a and b of the ellipsoid were determined using quasi-optical formulae [11] to focalize the output microwave beam into a 63.5 mm diameter HE_{11} corrugated waveguide.

After the grating, the output beam was reflected by a smooth plane mirror in order to reach the quartz window. The parameters of the cavity and the grating are summarized on Table II. The depolarization and distorsion losses associated to the curvature of the grating [12] are proportional to $(w_m/f)^2$ where w_m is the spot-size on the grating and f the focal length of the ellipsoid, and are negligible in our case ($< 0.1\%$).

An estimate of the ohmic losses on the grating was found by comparing the case of a grooved surface to the case of a smooth reflector. The presence of the grooves gives rise to a modulation of the surface current j_s associated with the reflection of the incident wave. The current distribution $j_s(r)$ was obtained from the electromagnetic theory of gratings [7] and is represented on Fig.4. For the grating used in our experiment, the maximum of $j_s(r)$ does not exceed the value corresponding to a plane reflector by more than 50% and the average heat load over one period of the grating is only 15% larger.

B. Diagnostics

Pattern measurements were performed by means of two different methods. The simplest one consisted in inserting a thin absorbing screen (Macor, liquid crystal paper or microwave absorber) in front of the window and recording the temperature increase with an IR camera. Since the temperature could be measured in real-time, this technique provided a good way of optimizing the alignment of the cavity, but on the other hand it was insensitive to either the polarization or the frequency.

The other scheme is shown on Fig.3. The microwave beam was attenuated by about -50 dB through a 4 cm layer of octanol ($C_8H_{18}O$). The power was collected by a WR-10 horn placed on a bidimensional translation stage. A set of directional couplers and attenuators allowed the simultaneous measurements of the frequency spectrum, the total RF power and the pattern of a single longitudinal mode. For the last option, the signal was fed into the RF input of a fundamental (f_{LO}=82 GHz) mixer. The IF signal was amplified (+60 dB) and then fed into a 16-channels multiplexer and a serie of narrowband filters ($\Delta f = 300$ MHz) with central frequencies regularly spaced between 8.2 GHz and 12.7 GHz. The frequency band covered by a single channel was comparable to the frequency separation between adjacent $TEM_{0,0,q}$ modes of the cavity ($\Delta f = 230$ MHz). The measurement of the pattern corresponding to a particular mode or the time evolution of the multimode competition could thus be recorded.

The cross-polarized content of the output beam was about the same order of magnitude as the polarization selectivity of the horn (-30 dB). In order to overcome this difficulty, a polarization discriminator was built. It consisted of an echelette grating designed in such a way that only the 0 and -1 orders of diffraction could propagate. The incidence angle and the echelette angle were selected to yield

$$e_{-1_{TE}} \simeq 0,\ e_{0_{TE}} \simeq 1$$
$$e_{-1_{TM}} \simeq 1, e_{0_{TM}} \simeq 0.$$

Using the fact that the grating acts as a smooth surface at order 0 together with the polarization discrimination of the horn made it possible to measure the cross-polarization pattern at order 0 of the echelette grating. A precise knowledge of the efficiencies (in this case

$e_{-1_{TE}} = 0.25$, $e_{0_{TE}} = 0.75$, $e_{-1_{TM}} < 0.01$ and $e_{0_{TM}} > 0.99$) gave the possibility of determining the fraction of output power in each polarization by measuring the power at orders 0 and -1 of the grating.

IV. RESULTS

A. Output pattern

An in-situ alignment of the cavity components was performed by optimizing the IR output pattern. This measurement was done at a low beam current to ensure a monomode emission. All the profiles presented here were made on a 10x10 points grid covering a surface of 10x10cm. Independent measurement with the high spatial resolution IR camera ensured that no fine structure was present. Fig.5 represents an output pattern measured at 22 cm of the window, at a frequency of 90.849 GHz, corresponding to the cavity mode $TEM_{0,0,393}$. The lines of equal power are separated by 2 dB. The measured spot-size of the beam (27.1 mm) is slightly larger than the computed one (20.4 mm). The gaussian content C^2 (Eq. 2) with a beam waist $w' = 27.1$ mm is 99.7%. Such a beam has a theoretical coupling coefficient into a HE_{11} waveguide of 97.4%. Also presented on Fig.5 are the profiles along a vertical line (A) and an horizontal line (B). The solid lines represent the best one dimensional gaussian fit. The beam size in the x-direction is 28.5 mm and in the y-direction 27.0 mm, indicating that the beam was symmetric at this location.

Since the phase of output wave could not be easily measured, the symmetry of output patterns taken at different locations was checked in order to make sure that the microwave output was an anastigmatic gaussian beam. The radiation pattern associated to the central mode was measured at 22 cm, 36 cm and 48 cm of the gyrotron window. The gaussian content (squares) and the spot-size (open circles) versus position are shown on Fig. 6. The continuous line represents the numerically computed width of the order 0 diffracted beam. The gaussian content C^2 found by optimizing the parameter w' is always larger than 95%. This result allows us to conclude that the output beam is truly gaussian. The same measurements also indicate that the output beam does not exactly focalize at the predicted point and that the beam waist was too large.

The cross-polarized pattern associated to the $TEM_{0,0,393}$ mode was measured using the polarization discriminator described in Sec. III and is presented on Fig.7, where the lines of equal power are separated by 0.5 dB. It is in good agreement with the numerical predictions [6], except for the presence of sidelobes. They can be due to spurious reflections (their effect was important in this case because of the low signal level) and to the fact that the incident wavefronts on the discriminator were not exactly plane and thus $e_{0_{TE}}$ was not constant over all the grating surface. A calorimeter was used to measure the power diffracted at the orders 0 and -1 of the discriminator. The measured fraction of depolarized power XP was less than 1% for all the cases.

Taking into account the larger experimental beam cross-section, the depolarization losses and using an ideal power coupling factor to the HE_{11} mode of a 2.5" diameter corrugated waveguide of 98% [13], it was estimated that the output beam of the central mode could be coupled to the HE_{11} mode with an efficiency of 94.5%. It should even be possible to increase this number up to 96% by having an output beam of ideal diameter [13].

B. Adjacent modes

A method for identification of the cavity modes in a QOG is to vary the mirror separation and to measure the change in the oscillation frequency. The experiment was performed by displacing the spherical mirror (the grating was not displaced in order to keep the output beam path fixed). Five modes were observed within a 4 mm change of the mirror separation and the frequency could be adjusted continuously within 600 MHz. The ouput patterns of the cavity modes $TEM_{0,0,394}$ and $TEM_{0,0,395}$ were measured. Their profile was similar to the central mode. However, their gaussian content was slightly lower ($> 95\%$), the beam was astigmatic ($w_x/w_y = 1.28$ for the mode $TEM_{0,0,394}$), and the direction of propagation was not exactly the same. At 22 cm from the window, the maximum of intensity of the mode $TEM_{0,0,394}$ was shifted by 5 mm with respect to the maximum of the central mode. These observations will be discussed in Sec. V.

C. Frequency tunability

It was pointed out in Ref. [8] that the frequency of the central mode could be adjusted by tilting the grating around its axis, in order to modify the angle of incidence, and thus the wavelength for which the Littrow condition is best fulfilled. The IR-pattern was optimized for two configurations of the grating. The difference in the incidence angle was approximately 0.5^o. In the first configuration (results presented before) the longitudinal index of the central mode was $q_0 = 393$ ($f \simeq 90.8$ GHz), whereas in the second configuration it was equal to 401 ($f \simeq 92.6$ GHz). Because of the rather cumbersome alignement procedure, no further investigation was made in this direction. The frequency tunability of this cavity set-up extends thus at least over 1.8 GHz.

D. Gyrotron performances

A set of experiment was performed in order to characterize the gyrotron behaviour and the specific features related to the use of a grating cavity. The quality factor of the $TEM_{0,0,q}$ modes of a Fabry-Pérot resonator formed by two spherical mirrors is essentially constant within the gyrotron instability bandwith [14], which is not the case for a diffraction grating cavity: the central mode and a few adjacent ones (typically 3 to 5) have a high quality factor ($Q = 61700$) and the latter decreases for other frequencies. Even though this feature cannot be considered as frequency selectivity, it allows the central mode to be preferentially excited in a grating cavity. The detuning

$$\delta\omega = 1 - \frac{\Omega_0}{\gamma\omega} \tag{7}$$

could thus be controlled by adjusting the magnetic field. The magnetic field was optimized for a few beam currents, as it is usually done with cylindrical gyrotrons [15]. It was previously not possible to carry out such an optimization on a QOG equipped with a conventional Fabry-Pérot resonator since a change of Ω_0 would lead to a mode jump, keeping the detuning approximately constant [16].

The result of such an optimization, performed on the present QOG, is shown on Fig.8. The circles represent the oscillation frequency and the triangles the interaction efficiency as a function of the static magnetic fied in the region of interaction, for a beam current of 10 A. The QOG oscillates in the central mode (f=90.8 GHz) over a magnetic field range $\Delta B/B$=1.5%, whereas in the case of a cavity formed by two spherical mirrors with the same mirror separation $\Delta B/B$ is reduced to 0.25% if the central mode is to be kept. The optimal magnetic field B_{opt} for beam currents up to 10 A is shown on Fig.9, where the open circles correspond to the experimental optima and the solid squares to multimode simulations in which the function $Q(f)$ as well as the beam voltage depression have been included. Both curves have the same qualitative behaviour, though the experimental measurement is systematically lower than the numerical prediction by 1%.

In previous QOG experiments, observations of simultaneous oscillation around the electron cyclotron frequency Ω_e and around $2\Omega_e$ have been reported [17], with a significant fraction of power emitted at the second harmonic. The grating used in the present experiment was designed such that no resonance could occur close to $2\Omega_e$. No oscillation around the second harmonic was detected, although the detection sensitivity was increased by 60 dB with respect to the one used at the fundamental. The use of a grating correctly designed has suppressed the harmonic competition in a QOG.

Represented on Fig.10 are the experimental maximum power (solid circles) and efficiency (solid squares) versus the beam current at optimal magnetic field, for an oscillation frequency of 90.8 GHz. The corresponding open symbols represent numerical predictions using a multimode simulation code. For currents above 7 A, the efficiency saturated at a value close to 14%, instead of the predicted 22%. The maximum efficiency was 15%, for a beam current I_b=13.5 A, corresponding to an output power of 150 kW. The lower than computed efficiency [16,18–20] is usually attributed to an increase of the velocity spreads of the electron beam.

V. DISCUSSION

A. Output beam size

It is shown in this section that the discrepancy between the experimentally measured output beam size and the theoretical prediction can be explained by the conjunction of a cavity misalignment and its operation at a frequency different from the design one. It is also qualitatively shown that the beam-wave interaction is relatively insensitive to these two factors.

Let us first consider the behavior of the grating as a function of the frequency. The grating profile is computed so that the Littrow condition is locally satisfied for the design frequency f_d everywhere on the grating for a bundle of rays issued from the focal point C_1 and converging to the focal point C_2 (see solid lines on Fig. 11). If the frequency does not exactly match the design one (the case $f < f_d$ is represented with dashed lines on Fig. 11), the bundles of rays satisfying the Littrow condition will form caustic surfaces which can be approximated at first order by two points C_1' and C_2'. By analogy with a conventional Fabry-Pérot resonator, the optical axis of the cavity is defined by the line passing through the center of curvature S of the spherical mirror and the focal point C_1'. In contrast to the Fabry-Pérot resonator, the grating resonator optical axis is now dependent on the frequency. As a

consequence, one resonant mode has minimal diffraction losses, whereas the optical axis of adjacent modes is tilted and the diffraction losses around the mirrors increase. This explains the existence of a central mode. In addition, spherical aberrations of the wavefronts related to the fact that the rays may intersect at a location different from the ellipsoid focal point also contribute to a decrease of the quality factors associated to adjacent modes.

A misalignment of one of the resonator components, such as a small tilt of either the grating or the spherical mirror has the effect of changing the relative location of S with respect to C_1'. The optical axis of the cavity is consequently affected, resulting in a shift in the frequency of the central mode.

A side-effect of the frequency dependency of the resonator optical axis is that the output microwave beam characteristics are also affected. Since the magnification associated with the ellipsoidal surface depends on the incidence point on the grating, not only the output waist location will change, but also its size.

In order to estimate qualitatively the magnitude order of the misalignment necessary to explain the experimental characteristics of the output beam, the equivalence of the grating cavity with a conventional Fabry-Pérot resonator was used. Knowing the design frequency f_d and the oscillation frequency f_o, the bundle of rays satisfying the Littrow condition on the grating for f_o could be graphically determined. The point C_1' was then set as the curvature center of the equivalent spherical mirror M_g. The curvature center S of the spherical mirror was then placed at arbitrary locations close to the design one and the characteristics of a $TEM_{0,0,q}$ resonant mode were determined using [14]:

$$w_{01} = \left(\frac{2D}{k}\right)^{\frac{1}{2}} \left(\frac{g_1 g_2 (1 - g_1 g_2)}{(g_1 + g_2 - 2 g_1 g_2)^2}\right)^{\frac{1}{4}} \tag{8}$$

where w_{01} is the waist of the cavity mode, D the mirror separation, $g_1 = 1 - D/R_s$ and $g_2 = 1 - D/R_g$ the curvature parameters, R_s and R_g the radii of curvature of the spherical mirror and the equivalent mirror respectively, and k is the wavenumber.

Returning to the ellipsoidal grating, the knowledge of the cavity gaussian-like beam properties allows to estimate the output beam waist location and size, using the well known quasi-optical propagation formulae [11].

The application of the above procedure indicates that a tilt of 0.5^o of the grating and a 2^o tilt of the spherical mirror can explain the measured spot-size at 22 cm of the window. These values are within the measurable accuracy of the position of the cavity components. Additionally, one finds that with a value of 0.5^o for the grating tilt, the location of the cavity beam waist remains very close to the electron beam and its size is almost equal to the design one (difference $< 1\%$). It can be concluded that, with our experimental parameters, the effect of the misalignment on the gyrotron interaction is negligible.

B. Gyrotron frequency and output power

The experimental optimal magnetic field was systematically smaller than the numerical prediction by about 1%. This discrepancy occured for all the currents at which the efficiency was optimized (see Fig.9) and cannot be accounted by an error in the determination of the

magnetic field. The explanation of this effect is not clear yet and a few hypotheses are suggested below.

Due to the coils configuration, the axial magnetic field B_z varies by 2% over the interaction gap. Gyrotron interaction at a location where B_z is higher than at the center of the gap can be expected if the resonator optical axis is shifted along the magnetic axis. According to multimode simulations, a longitudinal shift $\Delta z = 15$ mm of the cavity axis towards the gun might explain the discrepancy. This hypothesis was nevertheless discarded because in such a situation the electron beam tunnel would have intercepted the cavity mode (the distance between the beam duct edge and the resonator axis would have been 7 mm, compared to a spot-size of 10 mm) and substantially affected the output pattern.

A tilt of the resonator in a plane parallel to the electron beam can also introduce a frequency shift through the Doppler effect. Under our experimental conditions, a 2^o tilt leads to a shift of 1 GHz. Such a value appears unlikely because of the very good centering of the microwave beam with the output window. The plane reflector was mechanically aligned with an accuracy better than 0.5^o before the experiments and remained in a fixed position. An important observation lies in the experimental range Δq of excited longitudinal modes as a function of beam current, for a given set of conditions. The oscillation frequency (open circles) and the interaction efficiency (closed circles) at fixed parameters ($B_z = 3.53$ T, $V_k = 75$ kV, $\langle\alpha\rangle = 1.3$) are represented on Fig.12 as a function of the electron beam current I_b. The magnetic field corresponds to the experimental optimum for $I_b = 10$ A. The oscillation starts at low current in the mode $TEM_{0,0,387}$ at 89.3 GHz. The mode $TEM_{0,0,393}$ at 90.7 GHz is only excited for currents above 8 A and becomes the main mode at 9.5 A. The range of longitudinal modes indexes excited between the starting current and $I_b = 10$ A is thus $\Delta q_{exp} = 6$.

Monomode and multimode simulations, in which the actual magnetic field profile, beam depression and frequency dependence $Q(f)$ of the quality factor of modes $TEM_{0,0,q}$ are included, indicate that the maximal range of longitudinal modes excited between the starting current and 10 A is $\Delta q_{theo} = 4$. A possible explanation for the wider experimental range is that the electron beam suffers from a higher than predicted voltage depression, which affects the relativistic factor γ and thus the detuning. Assuming that the experimental conditions at 10 A correspond to the optimal detuning, it is estimated that an additional beam depression of 6.5 kV could explain the result. A multimode simulation performed with a beam energy decreased by a similar amount and keeping all other parameters constant revealed that the excitation of the mode $TEM_{0,0,393}$ was possible, with an interaction efficiency comparable to the experimental observation. A measure of the linear charge density performed in the drift section between the electron gun and the first hump of the magnetic field profile with a capacitive probe [21] corroborated this possibility. Depending on the gun parameters, the measured linear charge density could be as high as twice the predicted value, indicating the possible presence of a population of trapped electrons. The double-humped magnetic field configuration seems to be responsible for electron mirroring, since no charge excess was observed at low values of the electron beam pitch factor α. It has been shown in the case of cylindrical gyrotrons [22] that the modification of the electronic distribution function induced by electron trapping can strongly affect the beam depression and the gyrotron interaction, leading to an increase oscillation frequency.

VI. CONCLUSION

The possibility of producing a gaussian output pattern on a QOG by using an ellipsoidal grating as output coupler has been demonstrated. The gaussian content could be larger than 99%, with negligible depolarization losses (<1%). The power coupling factor to the HE_{11} mode of a corrugated waveguide was estimated to 94.5%. This value can potentially be increased up to 96% by optimizing the output beam size. The frequency tunability of the QOG and the coupling efficiency to an HE_{11} line might be affected by the sensitivity of the output beam spot-size to the cavity alignment, requiring the use of matching optics. The interaction length is nevertheless relatively insensitive to a misalignment.

An appropriate choice of the grating parameters allowed to suppress the presence of second harmonic oscillations. The frequency selectivity associated to the grating made it possible to optimize the static magnetic field, enhancing the interaction efficiency with respect to a QOG with a conventional Fabry-Pérot resonator.

Finally, it is suspected that a degradation of the electron beam properties and the presence of trapped electrons could be the cause of the reduced efficiency ($\eta \simeq 15\%$) and the discrepancy in the oscillation frequency at high currents.

VII. ACKNOWLEDGMENTS

This work was partially supported by the Office Fédéral de l'Energie under grants OFEN-EF-FUS(91)-01 and OFEN-Gyrotron 581 233, and by the Fonds National Suisse pour la Recherche Scientifique.

REFERENCES

* Present address: Plasma Fusion Center, Massachusetts Institute of Technology, Cambridge, 02139 MA.

[1] W. Kasparek, H. Kumrić, G.A. Müller, J. Pretterebner, P.G. Schüller and D. Wagner, Conceptual design of an Electron Cyclotron Wave system for ITER/NET, Final report, (1991).

[2] G.G. Denisov, A.N. Kuftin, V.I. Malygin, N.P. Venediktov, D.V. Vinogradov and V.E. Zapevalov, 110 GHZ gyrotron with a built-in converter, Int. J. Electronics, **72**, 1079 (1992).

[3] P. Sprangle, J.L. Vomvoridis and W.M. Manheimer, Theory of quasi-optical electron cycloton maser, Phys. Rev. A, **23**, 3127 (1981).

[4] J.P. Hogge, A.Perrenoud, M.Q. Tran, S. Alberti, B. Isaak, P. Muggli and T.M. Tran, Low power measurement of power coupling out of Fabry-Perot resonator at mm-wavelengths. Comparison between some techniques, Proc. Fourteenth Int. Conference on Infrared and Millimeter Waves, Würzburg 1989, **SPIE 1240**, 537 (1989).

[5] J.P. Hogge, H. Cao, W. Kasparek, T.M. Tran and M.Q. Tran, Output coupling of a quasi-optical Fabry-Perot resonator by mean of a diffractive grating in the mm wave region, Proc. Fifteenth Int. Conference on Infrared and Millimeter Waves, Orlando (Florida) 1990, **SPIE 1514**, 535 (1990).

[6] M.Q. Tran, H. Cao, J.Ph. Hogge, W. Kasparek, T.M. Tran and P.J. Paris, Properties of diffraction gratings used as output couplers in quasi-optical gyrotrons,J. Appl. Phys. **76**, 4056 (1982).

[7] R. Petit, Electromagnetic Theory of Gratings, Topics in Current Physics **22**, Springer-Verlag (1980).

[8] M. Roulin, M.Q. Tran and J.Ph. Hogge, Measurement of the Electric Field Pattern of a Fabry-Pérot Resonator Used in Quasi-Optical Gyrotrons, Int. J. Infrared and Millimeter Waves, **14**, 185 (1993).

[9] R. Gruber, S. Merazzi and T.M. Tran, DAPHNE: A programming environment for gyrotron optimization, Proc. Sixteenth Int. Conference on Infrared and Millimeter Waves, Lausanne 1991, **SPIE 1240,** 535 (1991).

[10] T.M. Tran, M.Q. Tran, S. Alberti, J.P. Hogge, B.Isaak, P. Muggli and A. Perrenoud, Prospects for High-Power Quasi-Optical Gyrotrons Operating in the Millimeter-Wave Range, IEEE Trans. on Electron. Devices II, **36**, 1983 (1989).

[11] P.F. Goldsmith, Quasi-optical Techniques at Millimeter and Submillimeter Wavelengths, Infrared and Millimeter Waves, **6**, 277, Academic Press (1982).

[12] J.A. Murphy, Distorsion of a simple gaussian beam on reflection from off-axis ellipsoidal mirrors, Int. J. Infrared and Millimeter Waves, **8**, 1165 (1987).

[13] L. Rebuffi and J.P. Crenn, Radiation patterns of the HE_{11} mode and gaussian approximations, Int. J. Infrared and Millimeter Waves, **10**, 291 (1989).

[14] A. Perrenoud, T.M. Tran, M.Q. Tran, C. Rieder and M. Schleipen, Open resonators for quasi-optical gyrotrons: structure of the modes and their influence, Int. J. Electronics, **57**, 985 (1984)

[15] B.G. Danly and R.J. Temkin, Generalized Nonlinear Harmonic Gyrotron Theory, Phys. Fluids, **29**, 561 (1986).

[16] S. Alberti, M.Q. Tran, J.P. Hogge, T.M. Tran, A. Bondeson, P.Muggli, A. Perrenoud, B. Jödicke, H.G. Mathews, Experimental measurements on a 100 GHz frequency tunable quasi-optical gyrotron, Phys. Fluids B, **2**, 1654 (1990).

[17] S. Alberti, M.Pedrozzi, M.Q. Tran, J.P. Hogge, T.M. Tran, P. Muggli, B. Jödicke and H.G. Mathews, Experimental measurements of competition between fundamental and second harmonic emission in a quasi-optical gyrotron, Phys. Fluids B, **2**, 2544 (1991).

[18] K.E. Kreischer, T.L. Grimm, W.C. Guss, A.W. Möbius and R.J. Temkin, Experimental study of a high-frequency megawatt gyrotron oscillator, Phys. Fluids B, **1**, 640 (1990).

[19] A.W. Fliflet, T.A. Hargreaves, W.M. Manheimer, R.P. Fischer and M.L. Barsanti, Initial operation of a high-power quasi-optical gyrotron, IEEE Trans. Plasma Science, **18**, 306 (1990).

[20] G. Gantenbein, E. Borie, G. Dammertz, O. Dumbrajs, M. Kuntze, H.-U. Nickel, B. Piosczyk and M. Thumm, 500 kW Operation of a 140GHz Gyrotron: Experiment and Simulation, Proc. Seventeenth Int. conference on infrared and millimeter waves, Pasadena 1992, **SPIE 1929** , 186 (1992).

[21] W.C. Guss, T.L. Grimm, K.E. Kreischer, J.T. Polevoy and R.J. Temkin, Velocity ratio measurements of a gyrotron electron beam, J. Appl. Phys., **69**, 3789 (1991).

[22] Sh.E. Tsimring, Limiting current of helical electron beams in gyrotrons, Int. J. Infrared and Millimeter Waves, **14**, 817 (1993).

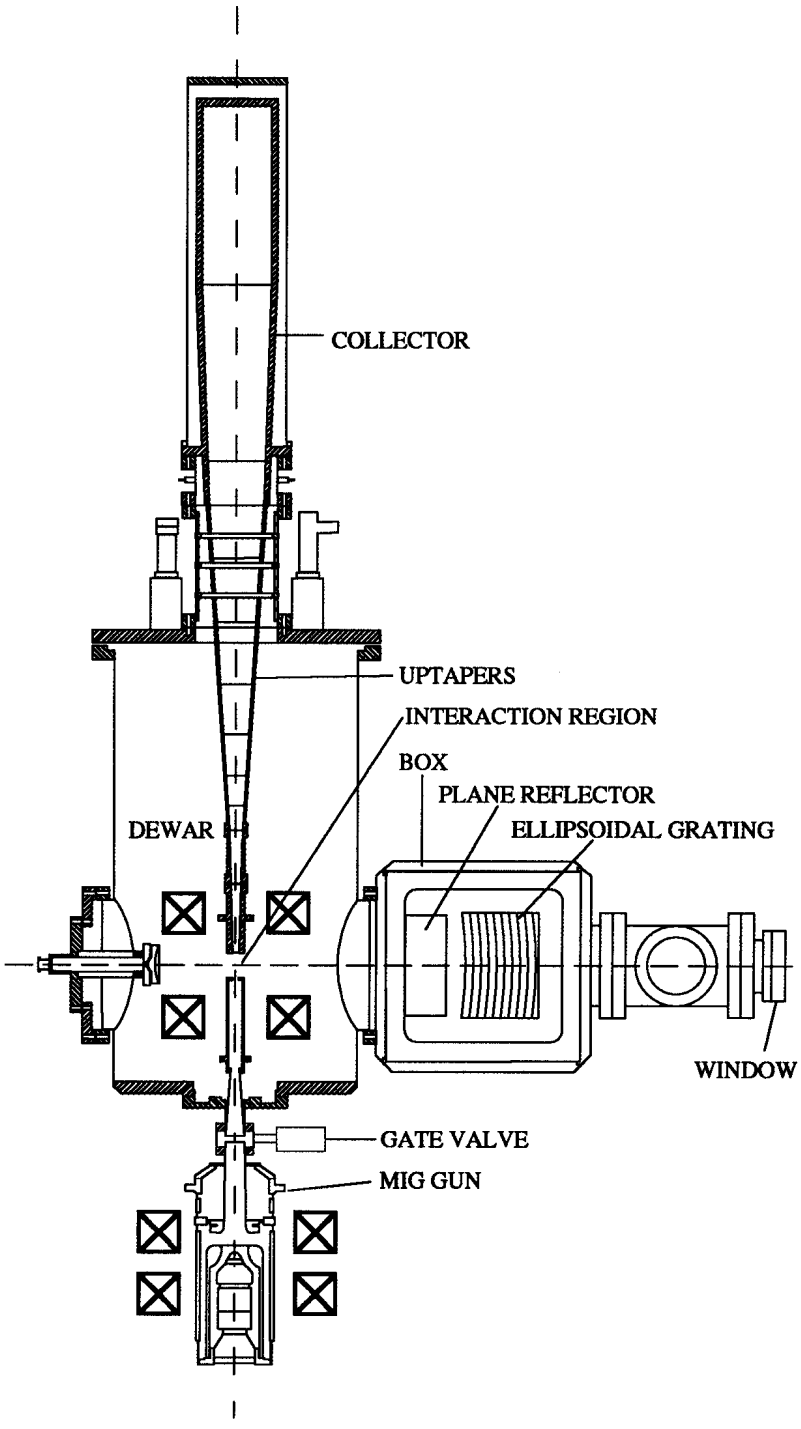

FIG. 1. Quasi-optical gyrotron, side-view.

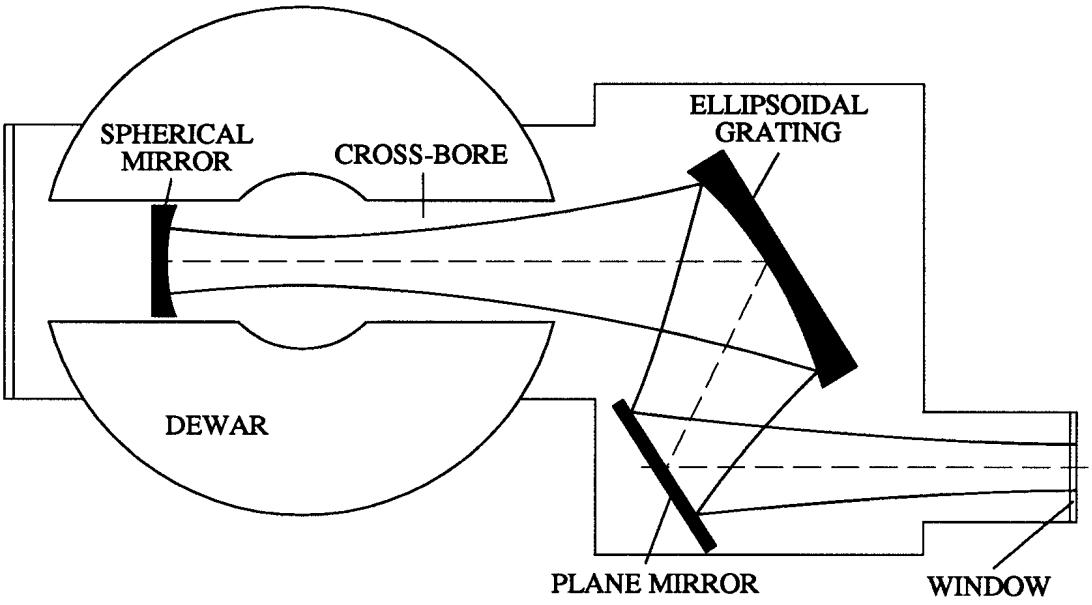

FIG. 2. Top-view of the cavity arrangment.

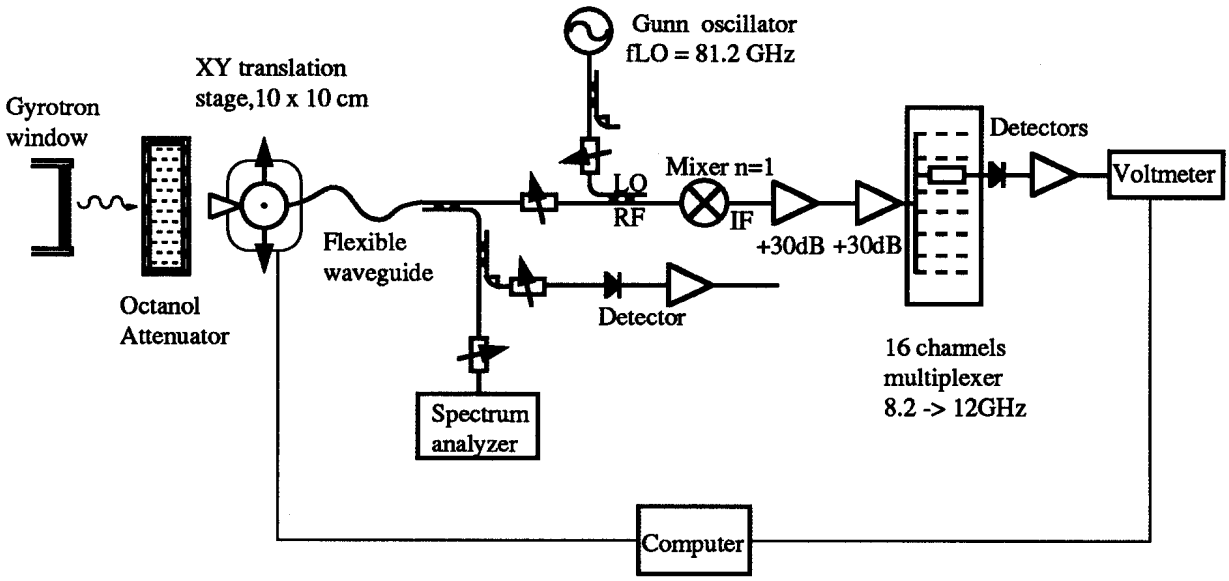

FIG. 3. Diagnostic of pattern, frequency and multimode evolution measurement.

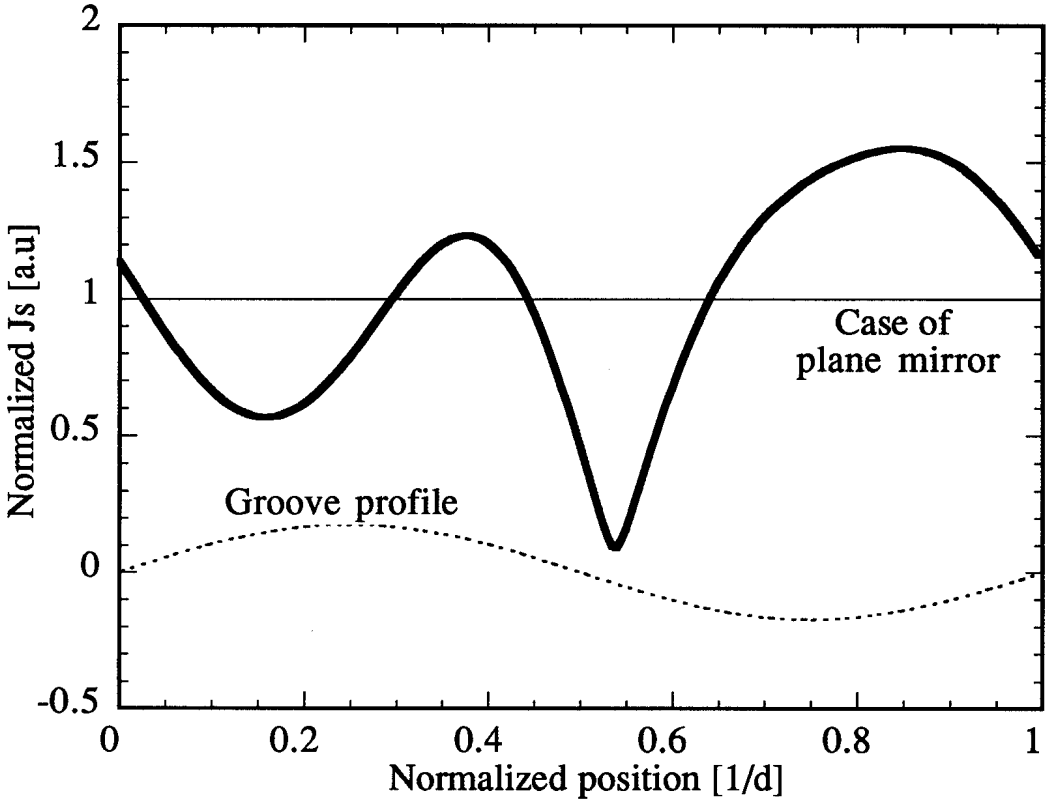

FIG. 4. Normalized amplitude of the surface current as a function of the position over one groove period. The value $j_s = 1$ corresponds to a smooth surface reflector. The parameters are: $h/d = 0.35$, $\lambda/d = 0.9389$,$\theta = 28$, TM polarization. The dashed line corresponds to the groove profile.

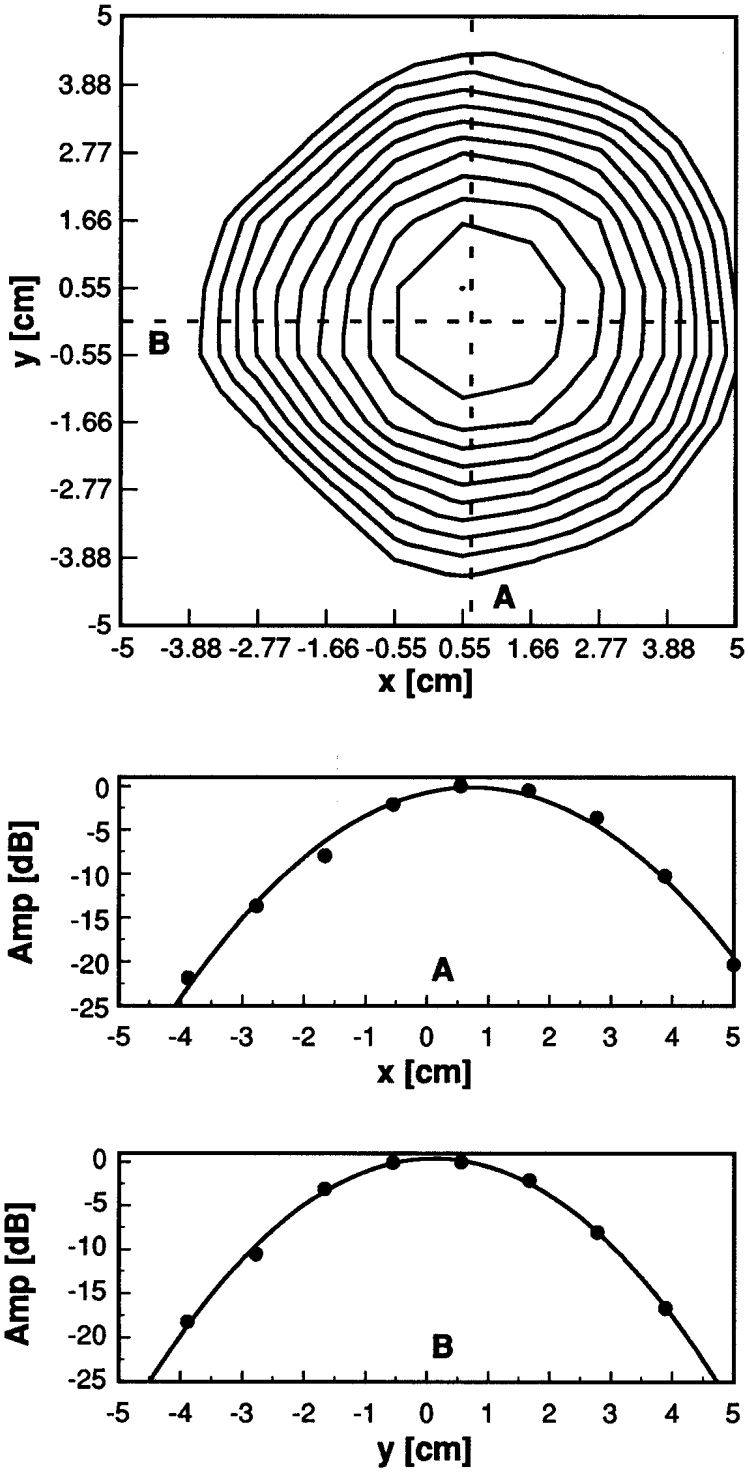

FIG. 5. Experimental output pattern of the gyrotron, measured at 22 cm of the window. The frequency is 90.849 GHz (mode $TEM_{0,0,393}$ of the cavity. Lines of constant power are separated by 2 dB. The highest gaussian content is $C^2 = 99.7\%$, obtained with $w' = 27.1$ mm. The profiles along a vertical line (A) and an horizontal line (B) (points) and the best 1-D gaussian fits (lines) are also presented. The beam size in the x-direction (y-direction) is 28.5 mm (27.0 mm).

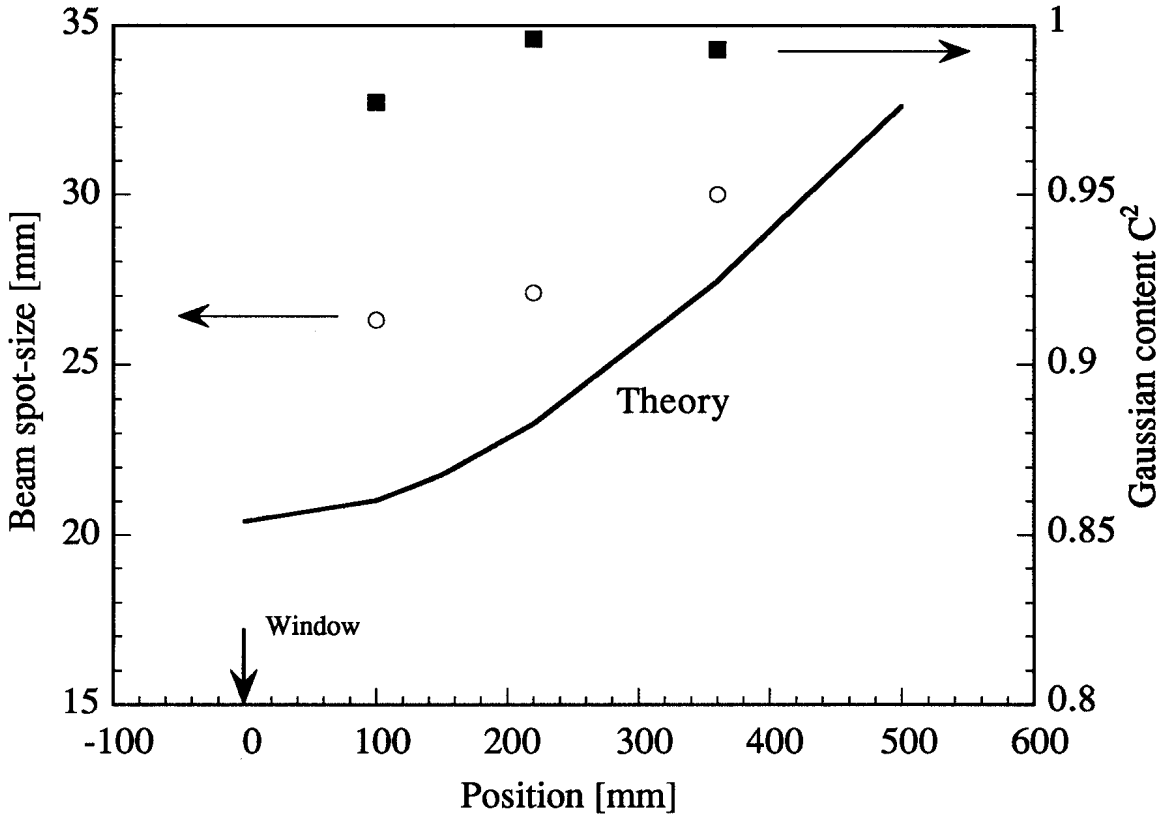

FIG. 6. Gaussian content (squares) and spot-size (open circles) of the radiation pattern associated to the central mode ($TEM_{0,0,393}$) versus the distance from the window. The continuous line represents the numerically computed size of the diffracted beam.

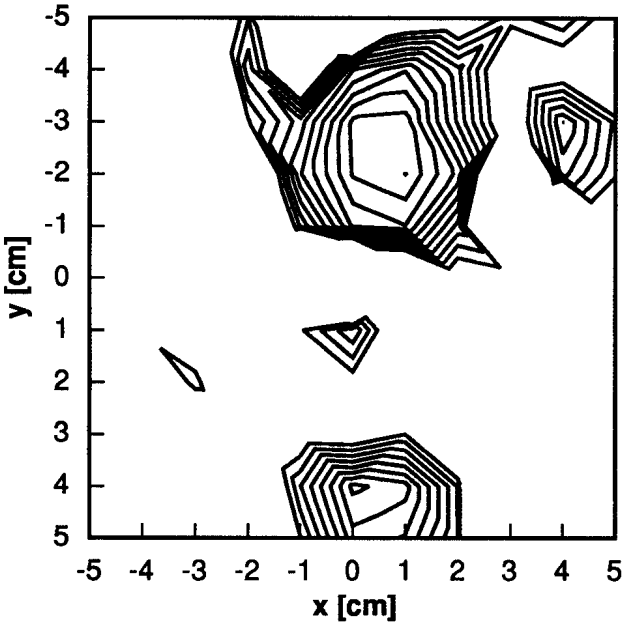

FIG. 7. Cross-polarized output pattern of the mode $TEM_{0,0,393}$, measured with the polarization discriminator. The lines of constant power are separated by 0.5 dB. The fraction of depolarized power is $XP < 1\%$.

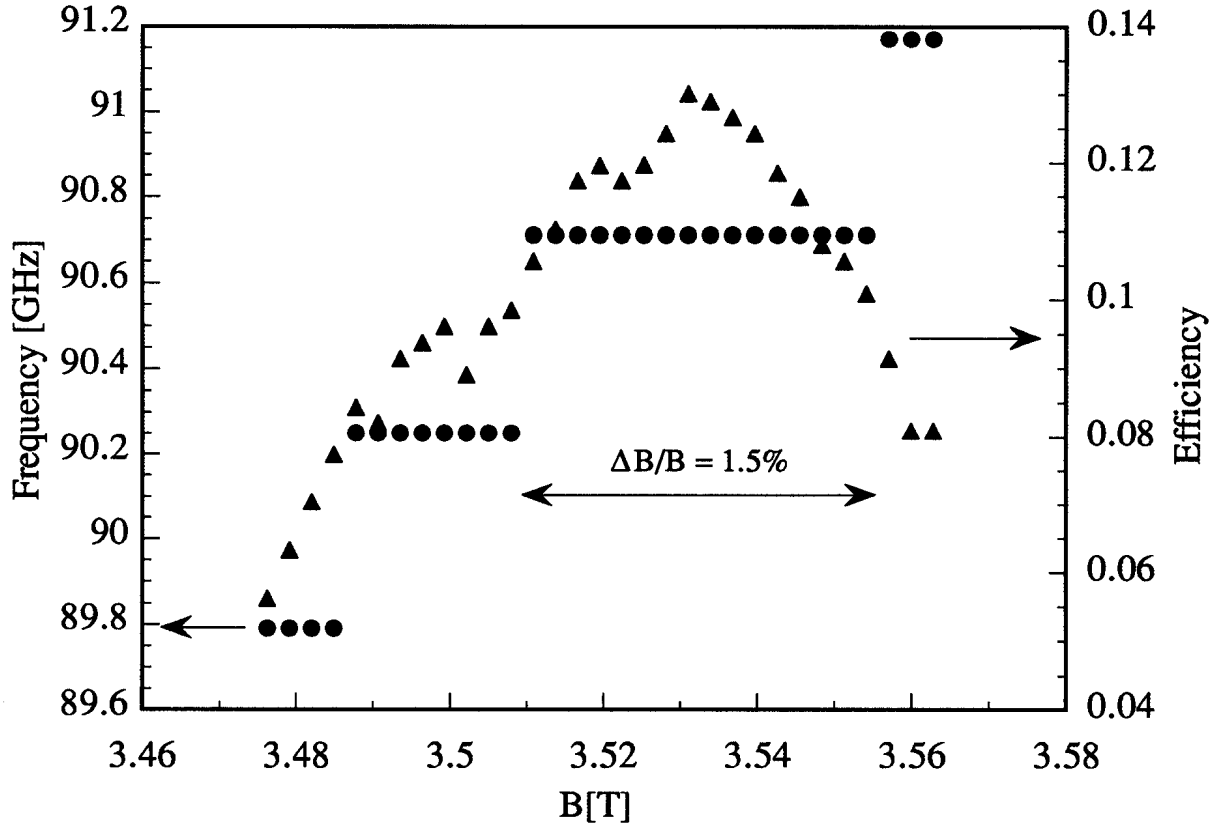

FIG. 8. Optimization of the magnetic field at I_b = 10 A, V_k=75 kV, $\langle\alpha\rangle$ = 1.3. The circles represent the oscillation frequency and the triangles the interaction efficiency.

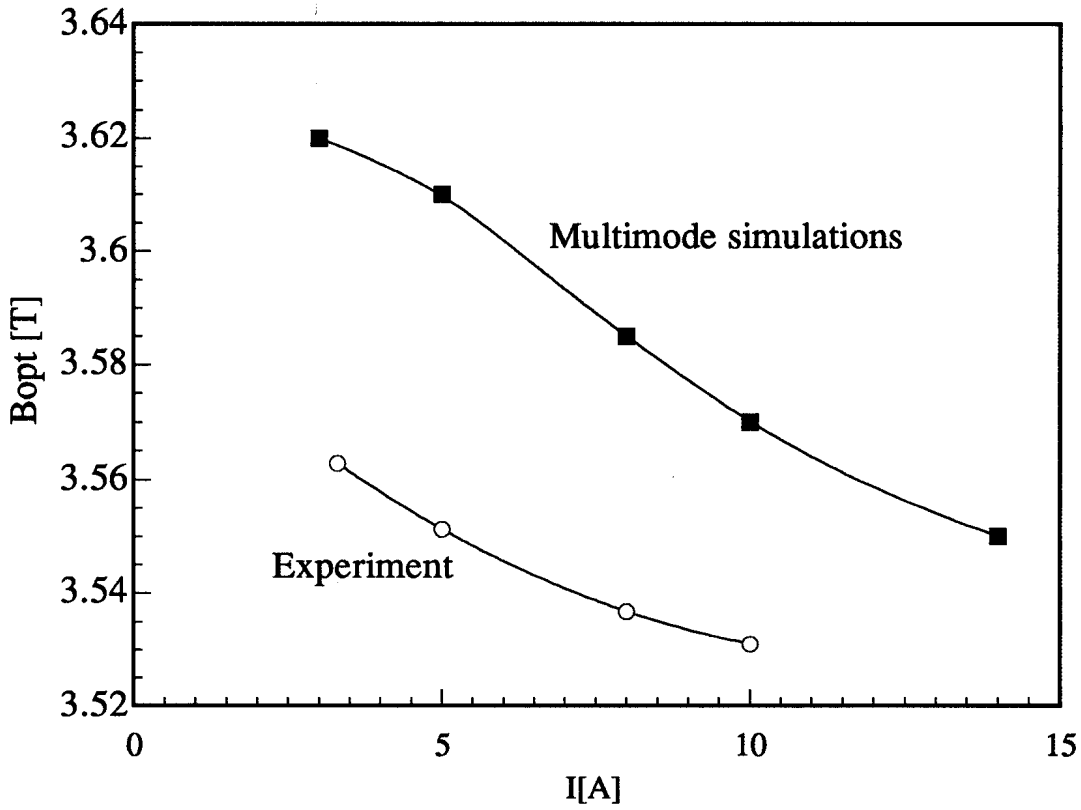

FIG. 9. Optimal magnetic field B_{opt} versus beam current I_b, for the mode $TEM_{0,0,393}$. Open circles: experimental values ($V_k = 75$ kV, $\langle\alpha\rangle = 1.3$), closed squares: multimode simulations in which the magnetic field profile, $Q(f)$ and the beam depression have been included.

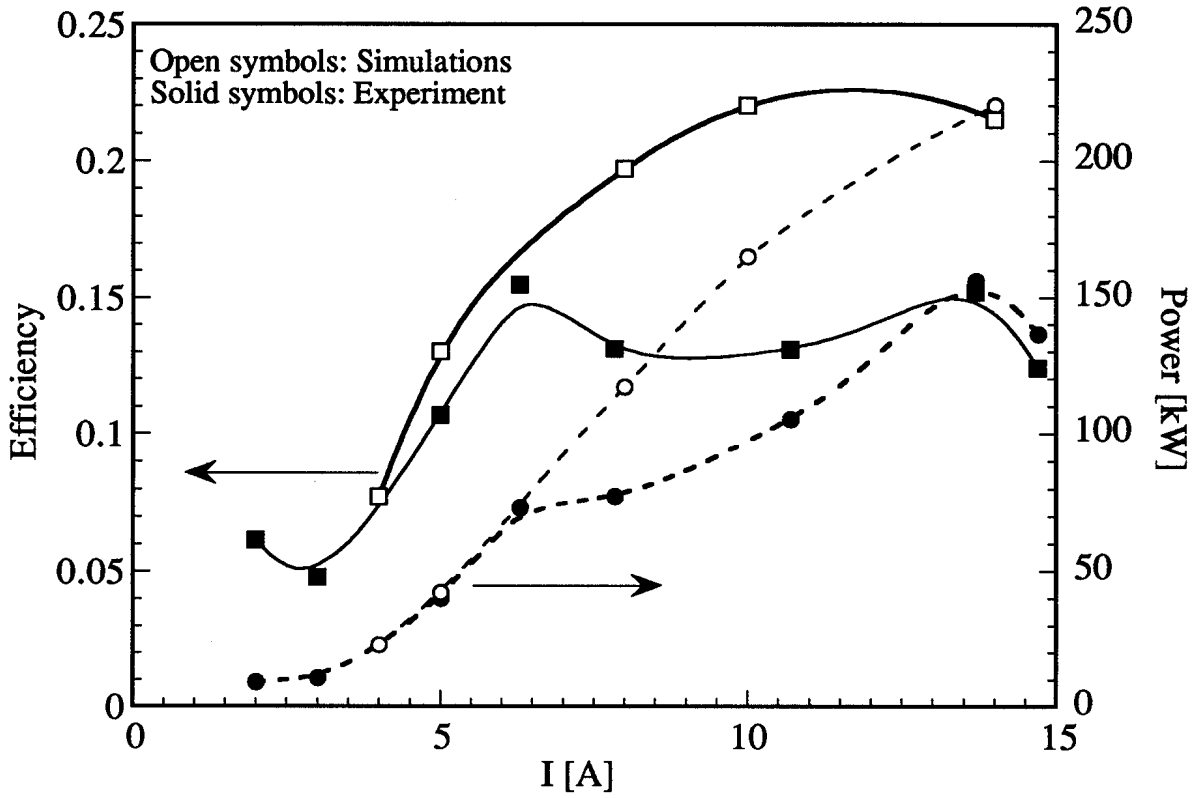

FIG. 10. Output power (circles) and efficiency (squares) at optimized magnetic field versus beam current I_b. Open symbols: multimode simulations, solid symbols: experimental measurements. The electron beam parameters are: $V_k = 75$ kV, $\langle\alpha\rangle = 1.3$

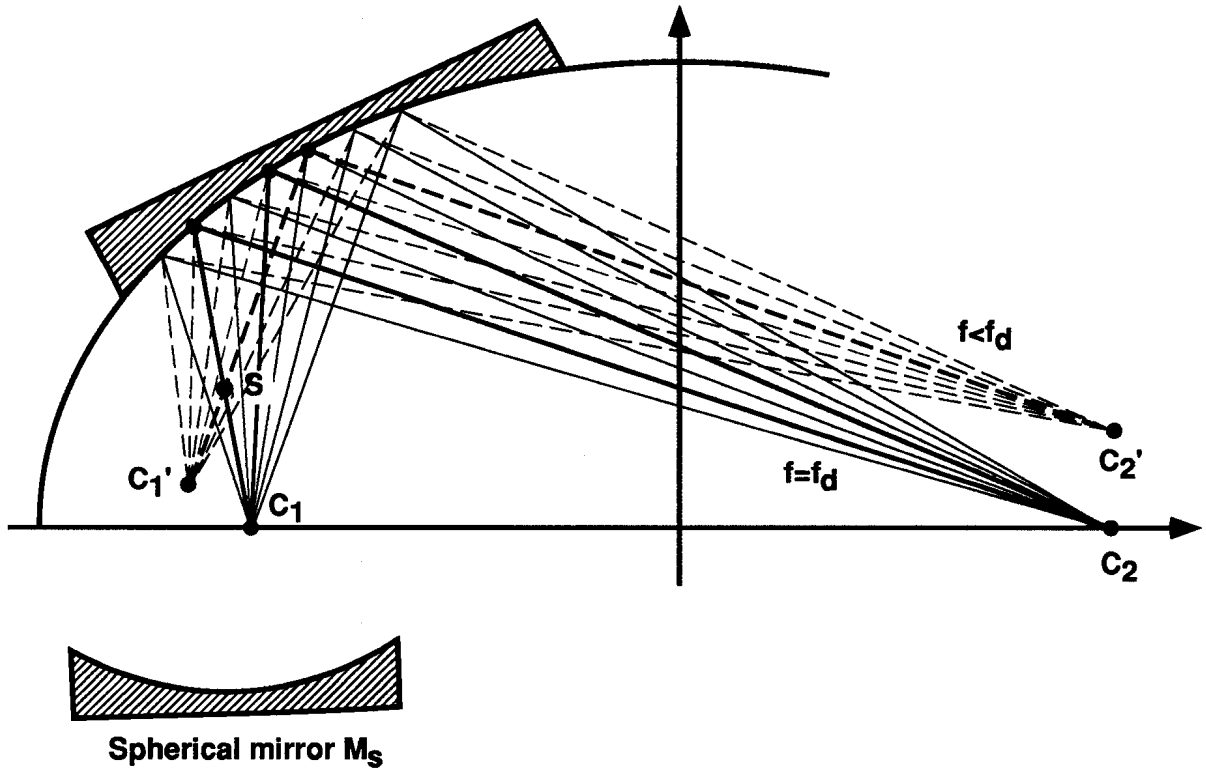

FIG. 11. Misalignment of the cavity. If $f = f_d$, the rays satisfying the Littrow condition (continuous lines) intersect on the focii C_1 and C_2 of the ellipsoid. The optical axis is given by the ray connecting C_1 and S, where S is the center of curvature of the spherical mirror. If $f \neq f_d$ (here $f_o < f_d$), the bundle of rays satisfying the Littrow condition (dashed lines) focalize on points C_1' and C_2'.

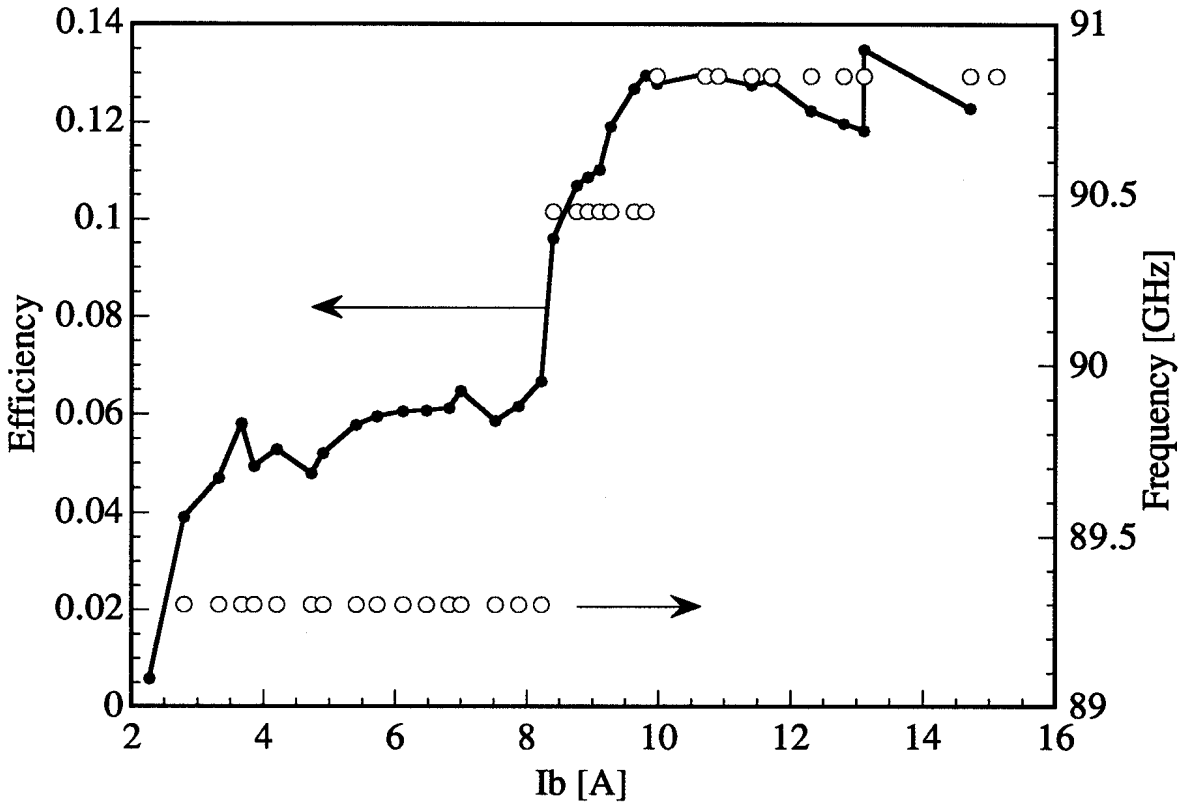

FIG. 12. Oscillation frequency (open circles) and interaction efficiency (line) versus beam current at fixed parameters. $B = 3.53$ T (experimental optimum at 10 A), V_k=75 kV, $\langle\alpha\rangle = 1.3$. The range of observed longitudinal modes is $\Delta q = 6$.

TABLES

TABLE I. Beam parameters in the interaction region, estimated with DAPHNE, for a cathode voltage of 75 kV, an anode voltage of 26 kV and a beam current of 14 A.

Parameter	Average value	Deviation
Beam radius	$\langle r_b \rangle = 3.33$ mm	$\frac{\Delta r_b}{\langle r_b \rangle} = 9.3\%$
Pitch angle	$\alpha \equiv \langle v_\perp / v_\parallel \rangle = 1.24$	$\frac{\Delta \alpha}{\langle \alpha \rangle} = 8.6\%$
Parallel velocity	$\langle \beta_\parallel \rangle = 0.295$	$\frac{\Delta \beta_\parallel}{\langle \beta_\parallel \rangle} = 5.4\%$
Perpendicular velocity	$\langle \beta_\perp \rangle = 0.365$	$\frac{\Delta \beta_\perp}{\langle \beta_\perp \rangle} = 3.7\ \%$
Relativistic factor	$\langle \gamma \rangle = 1.133$	$\frac{\Delta \gamma}{\langle \gamma \rangle} = 1\%$
Potential depression	6.8 kV	

TABLE II. Parameters of the cavity and the ellipsoidal grating.

Parameter	Value
Mirror separation D	650 mm
Dist. d_1 between beam waist and grating	500 mm
Incidence angle θ	28
Beam waist in cavity kw_{01}	20
Spot-size on grating kw_m	97
Beam waist of output beam kw_{02}	39.67
Design frequency	92.4 GHz
Longitudinal mode separation	230 MHz
Polarization	TM
Groove profile	sinusoidal
Groove depth h/d	0.35
Order 0 efficiency (TM) $e_{0_{TM}}$	4%
Order 0 efficiency (TE) $e_{0_{TE}}$	34%
Longitudinal index q	394
Quality factor Q	61700
Grating dimensions	300 x 200 mm
Spherical mirror diameter	74 mm
Curvature of spherical mirror	221.7 mm
Window	Quartz
Window diameter	100 mm
Semi-axis a of ellipsoid	808.6 mm
Semi-axis b of ellipsoid	667.4 mm
Curvature radius R_1 of incident beam	521.5 mm
Rayleigh length Z_{R_1} of incident beam	103.7 mm
Curvature radius R_2 of diffracted beam	1095.6 mm
Rayleigh length Z_{R_2} of diffracted beam	401.3 mm
Dist. d_2 grating - output beam waist	921 mm
Focal length f of ellipsoid ($\frac{1}{f} = \frac{1}{R_1} + \frac{1}{R_2}$)	353 mm
Ratio w_{01}/f	2.93 $\times 10^{-2}$
Magnification w_{02}/w_{01}	1.967